Silicon 1s Near Edge X-ray Absorption Fine Structure Spectroscopy of Functionalized Silicon Nanocrystals

A. Ritchie,[a] W. Cao,[a,1] M. Dasog,[b,2] T. K. Purkait,[b,3] C. Senger,[a] Y.F. Hu,[c] Q.F. Xiao,[c] J.G.C. Veinot,[b] and S.G. Urquhart[a]

a.) Department of Chemistry, University of Saskatchewan, Treaty Six Territory, Saskatoon, SK, S7N 0G6, Canada. Email: stephen.urquhart@usask.ca
b.) Department of Chemistry, University of Alberta, Edmonton, AB, T6G 2G2, Canada
c.) Canadian Light Source, University of Saskatchewan, Saskatoon, SK, S7N 2V3, Canada

1. Current address: Department of Physics, University of Oulu, Oulu, Finland
2. Current address: Department of Chemistry, Dalhousie University, Halifax, Canada, B3H 4R2
3. Current address: Department of Chemistry, Johns Hopkins University, Baltimore, MD, 21218, USA

Silicon 1s Near Edge X-ray Absorption Fine Structure (NEXAFS) spectra of silicon nanocrystals have been examined as a function of nanocrystal size (3 – 100 nm), varying surface functionalization (hydrogen or 1-pentyl termination), or embedded in oxide. The NEXAFS spectra are characterized as a function of nanocrystal size and surface functionalization. Clear spectroscopic evidence for long range order is observed Si-NCs that are 5-8 nm in diameter or larger. Energy shifts in the silicon 1s NEXAFS spectra of covalently functionalized silicon nanocrystals with changing size are attributed to surface chemical shifts and not to quantum confinement effects.

INTRODUCTION

Silicon nanocrystals (Si-NCs) have been widely investigated for their unique chemical and optoelectronic properties, as well as biocompatibility. As a result, several prototype applications such as light-emitting diodes, bioimaging, photovoltaics, sensing, batteries, and thermoelectrics have been demonstrated.[1-3] Many of these applications rely on Si-NC photoluminescence, conductivity and charge capacity that are highly dependent on Si-NC physical properties (particle size, crystallinity, surface chemistry, dopants, etc.). Si-NCs are optical emitters, and their crystallinity plays an important role in determining the photoluminescence maximum and quantum yields.[4-6] Their degree of crystallinity can also influence the Si-NC electrical[7-9] and thermal conductivity.[10] Although the effects of particle size and surface chemistry on Si-NC optoelectronic properties have been (and continue to be) investigated,[11-13] similar investigations of long-range crystallinity are more scarce.[14]

Near Edge X-ray Absorption Fine Structure (NEXAFS) spectroscopy is well-suited to provide information on electronic structure, structural order, strain, and surface functionalization for a wide variety of silicon based materials.[15-24] In the silicon 1s NEXAFS spectrum of crystalline silicon, a distinctive "rabbit ear" splitting is observed in the low energy intense band, the white line at ~1840 eV. Woicik *et al.* demonstrated that this white line splitting can be directly attributed to two strong peaks in the calculated conduction band density of states.[15] Furthermore, experimental trends in both the energy and relative intensities of the rabbit ear features track with the calculated peak splitting values[25] for crystalline silicon, silicon germanium alloys, and pure germanium.[15] The "rabbit ear" splitting was absent in the silicon 1s NEXAFS spectrum of amorphous silicon (produced *in situ*, and for which no low energy electron diffraction pattern was observed). Instead, a rounded white line was observed.[15] Based on this consistent experimental and computational evidence, Woicik *et al*. concluded that the "rabbit ear" feature in the silicon 1s NEXAFS spectra is an indicator of long range electronic order in silicon.[15] In this and subsequent work, the energy separation and relative intensity of the "rabbit ear" features was found to depend on alloy composition for SiGe alloys[17, 26] or the degree of lattice strain.[16, 17, 26] Recent high-quality Bethe-Salpeter calculations of the silicon 1s NEXAFS spectra reproduced this "rabbit ear" splitting.[27] The continuum of the Silicon 1s NEXAFS spectra of crystalline and amorphous silicon (~1850 – 2000 eV) is also sensitive to crystalline order, as multiple scattering effects lead to distinct features in spectra of crystalline samples.[28] However, this continuum will be obscured in the silicon 1s NEXAFS spectra of oxide embedded Si-NCs, as the strong SiO_2 contribution will obscure these weak features. The "rabbit ear" feature is more suitable for studies of long range order in Si-NCs.

Changes in the relative intensity of the conduction band splitting peaks in silicon 1s NEXAFS spectra have had broad utilization in measuring strain in crystalline silicon and silicon germanium alloys.[16, 17, 26] However, this "rabbit ear" splitting has not yet been reported in the silicon 1s NEXAFS spectra of nanocrystalline silicon materials (Si-NCs). Silicon 1s NEXAFS spectra of polydisperse[22, 23, 29] Si-NCs (formed by annealing of silicon rich SiO_2 / Si_3N_4 thin films) as well as Si-NCs with narrow size distributions have been examined,[18, 19] but in experiments with inadequate energy resolution to observe this splitting. In this work, the silicon 1s NEXAFS spectroscopy of Si-NCs are examined with an experimental energy resolution similar to the silicon 1s core-hole broadening (ca. 0.6 eV). Conduction-band splitting is observed in the NEXAFS spectrum of crystalline silicon measured at this energy resolution.

Several questions arise as we consider high resolution silicon 1s NEXAFS spectroscopy of Si-NCs:

- At what size threshold does the electronic structure of Si-NCs transform from a localized molecular description to a band-structure description?
- How does the fraction of surface and bulk states affect the NEXAFS spectra of Si-NCs as a function of size?
- Are quantum confinement effects revealed by NEXAFS spectroscopy of Si-NCs?

We note that the terms band structure and conduction band splitting may not be appropriate descriptors to interpret the NEXAFS spectra of very small Si-NCs. Such small Si-NCs may be better described as large molecules.

This paper explores the silicon 1s NEXAFS spectra of Si-NCs with a range of diameters (3-15 nm and 100 nm), different surface functionalities (hydrogen or 1-pentyl terminated), or embedded in oxide. Conduction band splitting, characteristic of long range order, is observed for Si-NCs particles 5-8 nm diameter or larger. Spectroscopic energy shifts for Si-NCs with different surface termination are also observed and characterized.

EXPERIMENTAL

SILICON NANOCRYSTALS

Materials: Hydrogen silsesquioxane (HSQ) was purchased from Dow Corning Corporation as a solution in methyl isobutyl ketone (FOx-17). Hydrofluoric acid (HF, 49% solution) was purchased from J. T. Baker (Univ. Alberta) or Merck (Univ. Saskatchewan). Borane-tetrahydrofuran complex (BH_3·THF, 1M solution

in THF), anhydrous toluene, methanol (ACS grade), ethanol (ACS grade), and 1-pentene (98%) were purchased from Sigma Aldrich and used without further purification.

Synthesis of oxide embedded silicon nanocrystals:

Oxide-embedded Si-NCs (Si-NCS in SiO_2) were prepared using the previously developed procedure.[30] Solid HSQ (~ 4 g) was transferred to a quartz boat and heated in a Lindberg Blue tube furnace from ambient temperature to peak processing temperature of 1100 °C at 18 °C /min under reducing atmosphere (5% H_2/95% Ar). The sample was maintained at 1100 °C for an hour, followed by cooling to the room temperature. The resulting brown solid was ground using an agate mortar and pestle. This method yields oxide-embedded Si-NCs with an average diameter of ca. 3 nm.

To obtain larger Si-NCs, the 3 nm Si-NC composite was transferred to a carbon boat and heated to 1200, 1300, 1400, or 1700 °C at 10 °C /min in a high temperature furnace (Sentro Tech Corp.) and maintained at the predetermined temperature for an hour under Ar atmosphere to yield ca. 5, 8, 14, and 100 nm particles, respectively. The composite was cooled to room temperature and stored in glass vials until further use. Crystal sizes were determined by applying the Scherrer analysis to X-ray diffraction lineshapes.[31] This method was found to be reliable for determining the diameter of Si-NC particles.[30]

Synthesis of hydrogen terminated silicon nanocrystals

Free standing hydrogen terminated Si-NCs (H-Si-NCs) were obtained by treating 100 mg of the Si-NC/SiO_2 composite of choice with 3 mL of 1:1:1 mixture of water, ethanol, and 49% HF for an hour in a PTFE vial in subdued light (Caution: Hydrofluoric acid is extremely dangerous and must be handled with great care.). The hydrophobic H-Si-NCs were extracted using two portions of 0.5 mL toluene. All remaining HF was neutralized using a saturated calcium chloride solution. The Si-NC/toluene mixture was centrifuged at 4000 rpm for 15 minutes and the toluene supernatant was decanted leaving a precipitate of H-Si-NCs. The particles were washed with toluene twice and stored under inert atmosphere until further use (typically less than 4 hours for NEXAFS spectroscopy measurements). The absence of oxide peaks in their silicon 1s NEXAFS spectra indicates that these materials were examined before significant oxidation could occur. The hydrogen terminated Si-NCs samples used in this work were obtained by etching the same oxide embedded Si-NCs source materials used for NEXAFS studies.

Synthesis of 1-pentyl-terminated silicon nanocrystals

1-pentyl terminated Si-NCs (1-pentyl Si-NCs) were prepared using a previously described method.[32] Freshly etched H-Si-NCs with the desired average diameter (ca. 3, 5, 8-9, 14, and 100 nm) were dispersed in dry toluene (ca. 5 mL) and degassed by three freeze-pump-thaw cycles using an Ar charged Schlenk line. Degassed 1-pentene (ca. 20 mmol) was added to the degassed H-Si-NC suspension. BH_3·THF solution (0.5 mol, 0.5 mL, 1M solution in THF) was added slowly to the solution using a syringe at 0 °C under Ar. The reaction mixture was stirred at room temperature for at least 12 hours. The resulting reaction mixture was transferred to a 50 mL PFE centrifuge tube and methanol (35 mL) was added. The mixture was centrifuged at 12,000 rpm for 30 min, and then the supernatant decanted and discarded. The pellet was dispersed in 3 mL toluene with sonication, and then an additional ca. 35 mL of methanol was added. This mixture was sonicated then centrifuged at 12,000 rpm for 30 min. The process was repeated once more. Finally, the purified 1-pentyl Si-NCs were dispersed in dry toluene until cast for use. The absence of oxide peaks in their silicon 1s NEXAFS spectra indicates that these materials were examined before significant oxidation could occur.

NEXAFS SPECTROSCOPY

Silicon 1s NEXAFS spectra were obtained at the Canadian Light Source (CLS) on the Soft X-ray Microcharacterization Beamline (SXRMB),[33] using a InSb(111) crystal monochromator. This monochromator configuration provides an energy resolution of 0.6 eV at the silicon 1s edge region. The silicon 1s NEXAFS spectra were recorded in total electron yield, and normalized by dividing each spectrum by an Io spectrum recorded simultaneously from an ion chamber upstream of the sample cell. The energy scale of the silicon 1s spectra was calibrated by setting the inflection point in the silicon 1s NEXAFS spectrum (obtained from the derivative) of HF etched crystalline silicon to 1839.2 eV.[26, 34] Samples of Si-NCs embedded in SiO_2 were mounted on silicon-free conductive carbon tape. Samples of H-Si-NCs and 1-pentyl Si-NCs were drop cast from solvent onto aluminium foil covered sample holders.

RESULTS

Figure 1 presents the low energy white-line band in the silicon 1s NEXAFS spectra of hydrogen-terminated silicon nanocrystals (H-Si-NCs; top), 1-pentyl terminated silicon nanocrystals (1-pentyl Si-NCs; middle) and oxide embedded silicon nanocrystals (Si-NCs in SiO_2; bottom). The silicon 1s NEXAFS

spectrum of a freshly HF etched silicon wafer is included for comparison. The extended energy range silicon 1s spectra of the oxide embedded Si-NCs are including in the Supplementary Material.

The characteristic “rabbit ear” conduction band splitting at ~1840 eV is clearly resolved in the spectrum of crystalline silicon (see *-marks in Figure 1) and in the spectra of the larger Si-NCs (i.e., 14 and 100 nm diameter Si-NCs). A zoom-in of the “rabbit ear” features is presented in Figure 2. The “rabbit ear” splitting is clearly observed in the larger Si-NCs, with a clear maximum, minimum, and maximum in the white line shape. The relative intensity of the first and second feature differs between Si-NCs with different surface termination. As the Si-NC diameter decreases, the “rabbit ear” splitting changes from two clearly resolved peaks (for large diameter Si-NCs), to a flat-topped white line (for 5-8 nm diameter Si-NCs), and then to a rounded white line (for 3 nm diameter Si-NCs). The lack of “rabbit-ear” splitting and a rounded white-line for the smallest Si-NCs may arise as a result of differences in electronic structure, or these features may be obscured by the increase in the fraction of surface atoms in the smaller NCs.

Figure 3 presents a plot of the derivative of the silicon 1s NEXAFS spectrum of H and 1-pentyl terminated Si-NCs and the oxide embedded Si-NCs. The derivative shows the inflection point in the silicon 1s white line, and is therefore sensitive to small energy shifts. An energy shift is observed for the covalently terminated (H / 1-pentyl) Si-NCs samples; as the Si-NCs size decreases, the inflection is shifted to higher energy. The shift is larger for the hydrogen terminated Si-NCs than for the 1-pentyl Si-NCs. In contrast, the oxide embedded Si-NCs do not show any energy shift with NC size. Note that the H-Si-NCs and oxide embedded Si-NCs samples come from a common Si-NC synthesis. The differences between these oxide embedded / H-terminated Si-NCs are therefore due to differences in their surface/interface properties, as their bulk NC structure is common.

DISCUSSION

In the previous section, we observed that the energy of the inflection point in the silicon 1s NEXAFS white line changes with NC size for H- and 1-pentyl- terminated Si-NCs, but not for oxide embedded Si-NCs. “Rabbit ear” conduction-band splitting features characteristic of long range order appear in the silicon 1s NEXAFS spectra of covalent (H-/1-pentyl) terminated Si-NCs 8 nm diameter or larger, and in oxide embedded Si-NCs 5 nm diameter or larger. Spectroscopic trends are expected to originate in changing surface / bulk ratios with Si-NCs size, as well as the development of long-range electronic order

(band structure) once Si-NCs pass a certain size threshold. One might also expect an energy shift due to differences in quantum confinement.

The silicon 1s white-line feature represents electronic transitions from the silicon 1s orbital to the conduction band. An increase in the transition energy could reflect a shift of conduction band to higher energy, an increase in the silicon 1s binding energy, or both effects simultaneously. A shift of the conduction band to higher energy with decreasing NC size would be consistent with the "particle in a box" quantum confinement picture. Size dependent single particle photoluminescence and tunnelling spectra analysis of alkyl-functionalized Si-NCs show an increase in the photoluminescence energy and the tunnelling gap with decreasing Si-NC diameter, consistent with quantum confinement.[35] The shift in the silicon 1s NEXAFS white line to higher energy with decreasing NC size for the H-/1-pentyl Si-NCs could suggest quantum confinement, if not for the *lack* of a shift with size for the oxide embedded Si-NCs. Quantum confinement shifts should depend on size alone, and not on surface termination. If quantum confinement was responsible for these shifts, they would also be visible in the spectra of the oxide embedded Si-NCs particles. We note that the H-Si-NCs and the oxide embedded Si-NCs are from a common synthesis, and differ only in the surface environment. We therefore conclude that the silicon 1s NEXAFS white-line energy does not reveal quantum confinement effects for small Si-NCs.

A key difference between the H- and 1-pentyl- terminated Si-NCs and oxide embedded Si-NCs is the nature of the Si-NCs termination: covalent Si-H or Si-C bonds for the H- and 1-pentyl terminated species, and predominantly ionic Si-O bonds[36] for the oxide embedded Si-NCs. These bonding differences lead to different sensitivity to "shell" atoms for the different Si-NC species. Silicon atoms at the boundary layer between the elemental NC core and the SiO_2 shell will have between 1 and 3 silicon-oxygen bonds. Previous studies on this Si-NC system indicate that the interface between the NCs and the oxide matrix is abrupt.[18] The absence of intermediate oxides in the longer energy range NEXAFS spectra of the oxide embedded Si-NCs (see supplementary information) confirms that the interface is abrupt in these samples.

Surface shifts are known to contribute to the position and shape of the Silicon 1s white line.[37] For oxide embedded Si-NCs, the presence of silicon – oxygen bonds shifts the energy of the silicon 1s NEXAFS white line to higher energy as the silicon atom is progressively oxidized, from ~1840 eV for crystalline silicon, Si(O), to ~1846 eV for SiO_2, Si(IV) (see Supplementary information). Similar observations were made in silicon 2p NEXAFS spectroscopy of intermediate SiO_x suboxides (shift of ~1 eV per oxidation state)[38] and the silicon 2p and silicon 1s NEXAFS spectra of $Si(CH_3)_x(OCH_3)_{4-x}$ (x = 0, 4) molecules.[39] The

silicon 1s white line (at ~1840 eV) will not contain contributions from silicon atoms bonded to any number of oxygen atoms, as the NEXAFS transitions for these oxidized silicon atoms will be shifted to higher energy, above the ~1840 eV white line. The ~1840 eV white line feature will only contain the "core" elemental silicon contributions.

In contrast, surface silicon atoms in the hydrogen or 1-pentyl terminated Si-NCs are *covalently* bonded to these termination groups. The energy shifts with covalent H- or 1-pentyl termination are modest relative to shifts for ionic silicon – oxygen bonds. Variable photon energy silicon XPS studies of a methyl-terminated Si(111) surface show that the silicon 2p binding energy of silicon atoms bonded to methyl groups are shifted 0.3 eV to higher binding energy, relative to bulk silicon.[40] This is attributed to the higher Pauling electronegativity of carbon (2.55) relative to silicon (1.90), creating a slight increase in the electropositivity of silicon.[40] A similar trend is expected for surface silicon atoms on 1-pentyl and H-terminated Si-NCs. The silicon 1s binding energy of the surface functionalized silicon atoms will increase slightly as the inductive effect of the H / 1-pentyl groups makes these functionalized atoms slightly electropositive. An increase in fraction of covalently bonded surface states with decreasing Si-NCs diameter will broaden the white line and shift it slightly to higher energy. This prediction is consistent with the observed shifts in the white line transition with Si-NCs size. As shown in Figure 3, the white line shifts to higher energy for smaller H / 1-pentyl terminated Si-NCs.

The size threshold for the on-set of the rabbit ear conduction band splitting is a challenge to resolve. In H-/1-pentyl terminated Si-NCs, the higher fraction of surface states and modest surface shifts will broaden the white line, while the width of the white line will be unaffected for oxide embedded Si-NCs. The relative fraction of surface versus bulk states as a function of Si-NCs is presented in Figure 4 (top). This calculation assumes a 1.6 Å shell thickness, based on the length of a Si-O bond. As the silicon 1s NEXAFS spectroscopy probing depth (for total electron yield detection) is 70 nm,[41] the entire NC volume will be probed. For the smallest (3 nm diameter) NCs the core atom fraction is ~70%, so ~30% of the white line signal will come from shifted surface states. This decreases to ~18% surface states in the 5 nm diameter Si-NCs, and to ~28% in the 3 nm diameter Si-NCs. A simulation of the core-shell NEXAFS spectrum of Si-NCs reveals how these surface effects will obscure the "rabbit ear" splitting. Figure 4 (bottom) shows a simulation of the silicon 1s NEXAFS spectra of crystalline (c-Si) and amorphous (a-Si) silicon (digitized from ref. [15]) weighted at 30% a-Si to reflect the 'shell' in 3 nm Si-NCs. This simulation is performed with and without a 0.3 eV shift to reflect potential surface atom binding energy shifts. The "rabbit ear" feature of crystalline silicon is obscured in this simulation, as the top of the white line

remains flat. However, the similarity of the Silicon 1s NEXAFS spectrum of amorphous silicon spectrum[15] to that of 3 nm diameter Si-NCs suggests that there is a considerable amorphous fraction in the smaller Si-NCs, perhaps larger than the shell fraction hypothesized above.

The oxide embedded Si-NCs NEXAFS spectra are more illuminating. As described above, the white line will not contain signal from the partially oxidized shell, so it will not be broadened by interface states. As shown in Figure 2, hints of the "rabbit ear" features are arguably visible in the 5 nm diameter oxide embedded Si-NCs, while these are not observed in the covalently functionalized Si-NCs of this size (rounded peak for 5 nm H-Si-NCs and 1-pentyl Si-NCs, in Figure 2). Surface chemical shifts likely obscure the "rabbit ear" feature in smaller Si-NCs. The spectra of the oxide embedded Si-NCs indicate the persistence of long-range order and band-structure character in Si-NCs as small as the 5-8 nm diameter. In the silicon 1s NEXAFS spectra of 3 nm diameter oxide embedded Si-NCs, the white line feature is much broader than any of the larger Si-NCs. This spectroscopic differences might suggest decreased structural order in the 3 nm oxide embedded Si-NCs, relative to the other Si-NCs. However, when the 3 nm diameter oxide-embedded Si-NCs sample were etched to produce hydrogen terminated Si-NCs (top of Figure 2), the 3 nm diameter H-Si-NCS have a spectral shape consistent with larger NCs. Therefore, the broadness of the 3 nm diameter oxide embedded Si-NCs spectra is not due to disorder, but rather overlap of suboxide transitions occuring at higher energy.

CONCLUSIONS

High energy resolution silicon 1s NEXAFS spectra of Si-NCs have been examined as a function of NC size (3 – 15 nm; 100 nm), surface termination (H- or 1-pentyl) and for oxide embedded Si-NCs. "Rabbit ear" conduction band splitting in the silicon 1s white line are observed in Si-NCs for the first time. These features originate from conduction band splitting and are diagnostic of long range order.

Shifts in the energy of the silicon 1s white line with NC size are observed for H- and 1-pentyl terminated Si-NCs, but not for oxide embedded Si-NCs. The presence of small shifts in the spectra of covalently terminated NCs and their absence in the spectra of oxide embedded NCs is consistent with the magnitude of surface induced chemical shifts: small for covalent functionalization and large for ionic bonding. Our results clearly show that the silicon 1s NEXAFS spectra are insensitive to quantum confinement effects.

"Rabbit ear" features consistent with conduction-band splitting and long range order and the development of band structure are observed for oxide embedded Si-NCs with a diameter of 5 nm or greater, and for covalently terminated Si-NCs with a diameter of 8 nm or larger. These results indicate that Si-NCs with a diameter of 5-8 nm of greater can be described as having long range order.

SUPPLEMENTARY MATERIAL

See supplementary material for the long range silicon 1s NEXAFS spectra of oxide embedded Si-NCs.

ACKNOWLEDGEMENTS

SGU is funded by NSERC (Discovery and Strategic grants) and JV is funded by NSERC Discovery grant program. MD thanks Alberta Innovates Technology Futures, Killam Trusts, and NSERC for scholarships. Research described in this paper was performed at the Canadian Light Source, which is supported by the Canada Foundation for Innovation, Natural Sciences and Engineering Research Council of Canada, the University of Saskatchewan, the Government of Saskatchewan, Western Economic Diversification Canada, the National Research Council Canada, and the Canadian Institutes of Health Research.

FIGURE CAPTIONS

Figure 1: Silicon 1s NEXAFS spectra of hydrogen terminated silicon nanocrystals (top; H-Si-NCs), 1-pentyl terminated silicon nanocrystals (middle: 1-pentyl Si-NCs) and oxide embedded silicon nanocrystals (bottom; Si-NCs in SiO_2), of various diameter (3 nm, 5 nm, 8-9 nm, 14 nm and 100 nm). The silicon 1s NEXAFS spectrum of HF-etched crystalline silicon is included for comparison. The "rabbit ears" are the two peaks present in the 1840 – 1841.5 eV energy range. These are most clearly resolved in the spectrum of crystalline silicon, where they are indicated with asterisk symbols. Spectra have been offset for clarity.

Figure 2: Magnification of the 'rabbit ear' feature in the silicon 1s NEXAFS spectra of hydrogen terminated silicon nanocrystals (top; H-Si-NCs), 1-pentyl terminated silicon nanocrystals (middle: 1-pentyl Si-NCs) and oxide embedded silicon nanocrystals (bottom; Si-NCs in SiO_2), of various diameter (3 nm, 5 nm, 8-9 nm, 14 nm and 100 nm). Spectra have been offset for clarity.

Figure 3: Derivative of the silicon 1s NEXAFS spectra of hydrogen terminated silicon nanocrystals (top; H-Si-NCs), 1-pentyl terminated silicon nanocrystals (middle: 1-pentyl Si-NCs) and oxide embedded silicon nanocrystals (bottom; Si-NCs in SiO_2), of various diameter (3 nm, 5 nm, 8-9 nm, 14 nm and 100 nm).

Figure4: (top) Surface to bulk ratios in Si-NCs as a function of NC diameter, for Si-NCs with a 1.6 Å shell thickness. The circles represent Si-NCs diameters examined in this work. (bottom) Simulation of the silicon 1s NEXAFS spectra of crystalline silicon with a 30% amorphous component and with a 0.3 eV shifted 30% amorphous content. Crystalline silicon (c-Si) and amorphous silicon (a-Si) spectra were digitized from ref. [15].

REFERENCES

1. X. Cheng, S. B. Lowe, P. J. Reece and J. J. Gooding, Chemical Society Reviews **43** (8), 2680-2700 (2014).
2. M. Dasog, J. Kehrle, B. Rieger and J. G. C. Veinot, Angewandte Chemie International Edition **55** (7), 2322-2339 (2016).
3. S. P. Ashby, J. A. Thomas, J. Garcia-Canadas, G. Min, J. Corps, A. V. Powell, H. Xu, W. Shen and Y. Chao, Faraday Discussions **176** (0), 349-361 (2014).
4. R. Anthony and U. Kortshagen, Physical Review B **80** (11), 115407 (2009).
5. S. Askari, V. Svrcek, P. Maguire and D. Mariotti, Advanced Materials **27** (48), 8011-8016 (2015).
6. D. C. Hannah, J. Yang, N. J. Kramer, G. C. Schatz, U. R. Kortshagen and R. D. Schaller, ACS Photonics **1** (10), 960-967 (2014).
7. Z. H. Khan, Applied Surface Science **255** (21), 8874-8878 (2009).
8. Z. Shen, U. Kortshagen and S. A. Campbell, Journal of Applied Physics **96** (4), 2204-2209 (2004).
9. I. Alessia, I. Fabio, C. Isodiana, D. P. Calogero, F. Giorgia, B. Corrado, S. Delfo, S. Gianfranco Di, P. Angelo, F. Pier Giorgio, C. Andrea and P. Francesco, Nanotechnology **17** (5), 1428 (2006).
10. F.-L. Arthur, M. Samy, A. Tristan, L. David and T. Konstantinos, Journal of Physics: Condensed Matter **26** (35), 355801 (2014).
11. D. S. English, L. E. Pell, Z. Yu, P. F. Barbara and B. A. Korgel, Nano Letters **2** (7), 681-685 (2002).
12. X. Li, Y. He, S. S. Talukdar and M. T. Swihart, Langmuir **19** (20), 8490-8496 (2003).
13. M. Dasog, G. B. De los Reyes, L. V. Titova, F. A. Hegmann and J. G. C. Veinot, ACS Nano **8** (9), 9636-9648 (2014).
14. V. Petkov, C. M. Hessel, J. Ovtchinnikoff, A. Guillaussier, B. A. Korgel, X. Liu and C. Giordano, Chemistry of Materials **25** (11), 2365-2371 (2013).
15. J. C. Woicik, R. S. List, B. B. Pate and P. Pianetta, Solid State Communications **65** (7), 685-688 (1988).
16. W. Cao, M. Masnadi, S. Eger, M. Martinson, Q. F. Xiao, Y. F. Hu, J. M. Baribeau, J. C. Woicik, A. P. Hitchcock and S. G. Urquhart, Applied Surface Science **265**, 358-362 (2013).
17. A. P. Hitchcock, T. Tyliszczak, P. Aebi, X. H. Feng, Z. H. Lu, J. M. Baribeau and T. E. Jackman, Surface Science **301** (1-3), 260-272 (1994).
18. C. M. Hessel, E. J. Henderson, J. A. Kelly, R. G. Cavell, T.-K. Sham and J. G. C. Veinot, The Journal of Physical Chemistry C **112** (37), 14247-14254 (2008).
19. J. A. Kelly, E. J. Henderson, R. J. Clark, C. M. Hessel, R. G. Cavell and J. G. C. Veinot, The Journal of Physical Chemistry C **114** (51), 22519-22525 (2010).
20. C. Euaruksakul, Z. W. Li, F. Zheng, F. J. Himpsel, C. S. Ritz, B. Tanto, D. E. Savage, X. S. Liu and M. G. Lagally, Physical Review Letters **101** (14), 147403 (2008).
21. C. Euaruksakul, F. Chen, B. Tanto, C. S. Ritz, D. M. Paskiewicz, F. J. Himpsel, D. E. Savage, Z. Liu, Y. Yao, F. Liu and M. G. Lagally, Physical Review B **80** (11), 115323 (2009).
22. L. J. Borrero-González, L. A. O. Nunes, F. E. G. Guimarães, J. Wojcik, P. Mascher, A. M. Gennaro, M. Tirado and D. Comedi, Journal of Physics: Condensed Matter **23** (50), 505302 (2011).
23. P. R. Wilson, T. Roschuk, K. Dunn, E. N. Normand, E. Chelomentsev, O. H. Zalloum, J. Wojcik and P. Mascher, Nanoscale Res Lett **6** (1), 168 (2011).
24. J. A. Kelly, E. J. Henderson, C. M. Hessel, R. G. Cavell and J. G. C. Veinot, Nuclear Instruments and Methods in Physics Research Section B: Beam Interactions with Materials and Atoms **268** (3–4), 246-250 (2010).
25. D. J. Stukel, Physical Review B **3**, 3347 (1971).

26. A. P. Hitchcock, T. Tyliszczak, P. Aebi, J. Z. Xiong, T. K. Sham, K. M. Baines, K. A. Mueller, X. H. Feng, J. M. Chen, B. X. Yang, Z. H. Lu, J. M. Baribeau and T. E. Jackman, Surface Science **291** (3), 349-369 (1993).
27. E. L. Shirley, J. A. Soininen and J. J. Rehr, Proceedings of the SPIE **5538**, 125 (2004).
28. A. Bianconi, A. Di Cicco, N. V. Pavel, M. Benfatto, A. Marcelli, C. R. Natoli, P. Pianetta and J. Woicik, Physical Review B **36** (12), 6426-6433 (1987).
29. P. R. Wilson, T. Roschuk, K. Dunn, E. Normand, E. Chelomentsev, J. Wojcik and P. Mascher, ECS Transactions **28** (3), 51-59 (2010).
30. C. M. Hessel, E. J. Henderson and J. G. C. Veinot, Chemistry of Materials **18** (26), 6139-6146 (2006).
31. J. I. Langford and A. J. C. Wilson, Journal of Applied Crystallography **11** (2), 102-113 (1978).
32. T. K. Purkait, M. Iqbal, M. H. Wahl, K. Gottschling, C. M. Gonzalez, M. A. Islam and J. G. C. Veinot, Journal of the American Chemical Society **136** (52), 17914-17917 (2014).
33. Y. F. Hu, I. Coulthard, D. Chevrier, G. Wright, R. Igarashi, A. Sitnikov, B. W. Yates, E. L. Hallin, T. K. Sham and R. Reininger, AIP Conference Proceedings **1234** (1), 343-346 (2010).
34. R. McGrath, I. T. McGovern, D. R. Warburton, D. Purdie, C. A. Muryn, N. S. Prakash, P. L. Wincott, G. Thornton, D. S. L. Law and D. Norman, Physical Review B **45** (16), 9327-9338 (1992).
35. O. Wolf, M. Dasog, Z. Yang, I. Balberg, J. G. C. Veinot and O. Millo, Nano Letters **13** (6), 2516-2521 (2013).
36. R. J. Gillespie and S. A. Johnson, Inorganic Chemistry **36** (14), 3031-3039 (1997).
37. J. C. Woicik, B. B. Pate and P. Pianetta, Physical Review B **39** (12), 8593-8604 (1989).
38. G. R. Harp, Z. L. Han and B. P. Tonner, Journal of Vacuum Science & Technology A **8** (3), 2566-2569 (1990).
39. D. G. J. Sutherland, M. Kasrai, G. M. Bancroft, Z. F. Liu and K. H. Tan, Physical Review B **48** (20), 14989-15001 (1993).
40. K. T. Wong and N. S. Lewis, Accounts of Chemical Research **47** (10), 3037-3044 (2014).
41. M. Kasrai, W. N. Lennard, R. W. Brunner, G. M. Bancroft, J. A. Bardwell and K. H. Tan, Applied Surface Science **99** (4), 303-312 (1996).

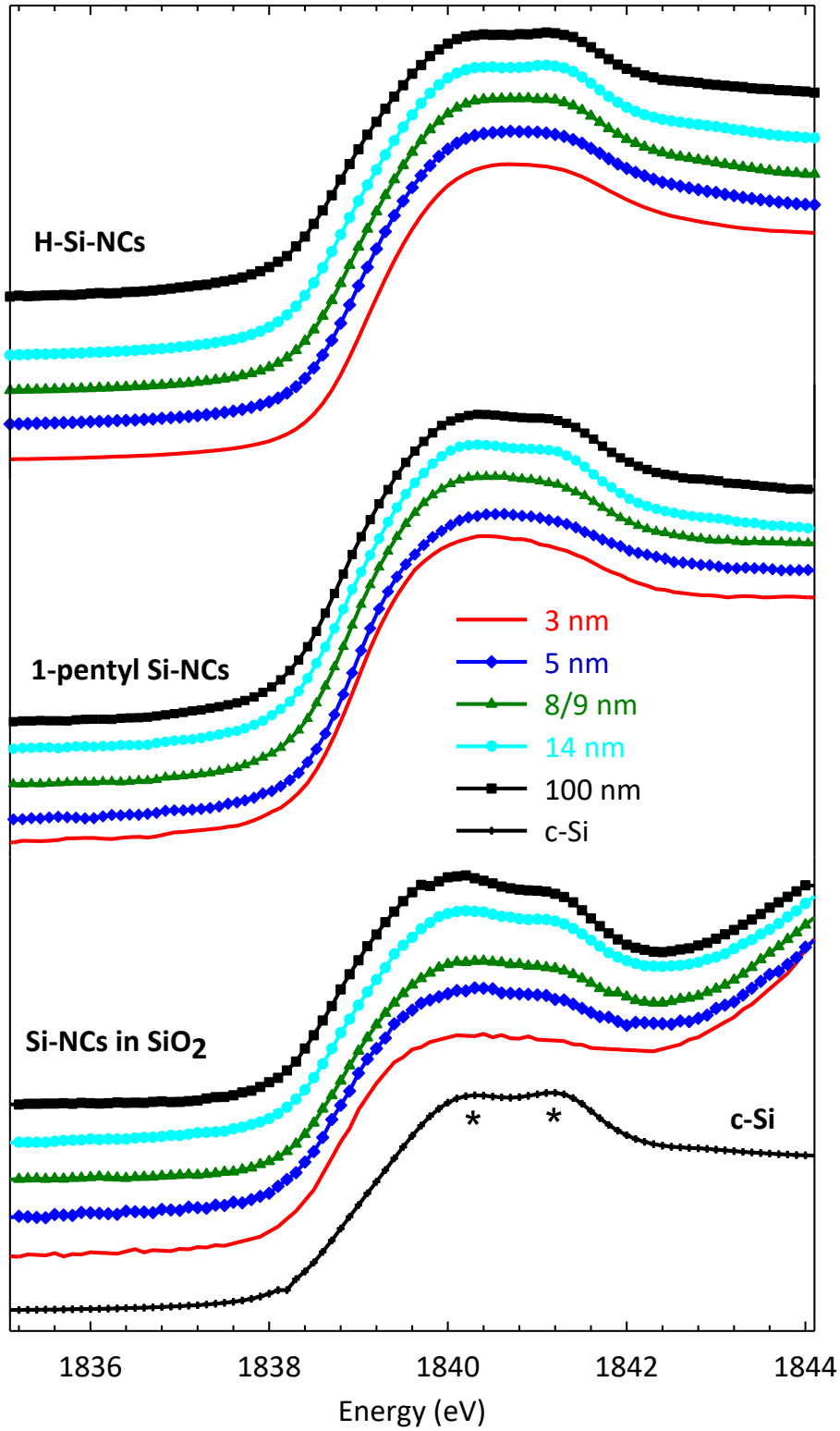

Figure 1: Silicon 1s NEXAFS spectra of hydrogen terminated silicon nanocrystals (top; H-Si-NCs), 1-pentyl terminated silicon nanocrystals (middle: 1-pentyl Si-NCs) and oxide embedded silicon nanocrystals (bottom; Si-NCs in SiO_2), of various diameter (3 nm, 5 nm, 8-9 nm, 14 nm and 100 nm). The silicon 1s NEXAFS spectrum of HF-etched crystalline silicon is included for comparison. The "rabbit ears" are the two peaks present in the 1840 – 1841.5 eV energy range. These are most clearly resolved in the spectrum of crystalline silicon, where they are indicated with asterisk symbols. Spectra have been offset for clarity.

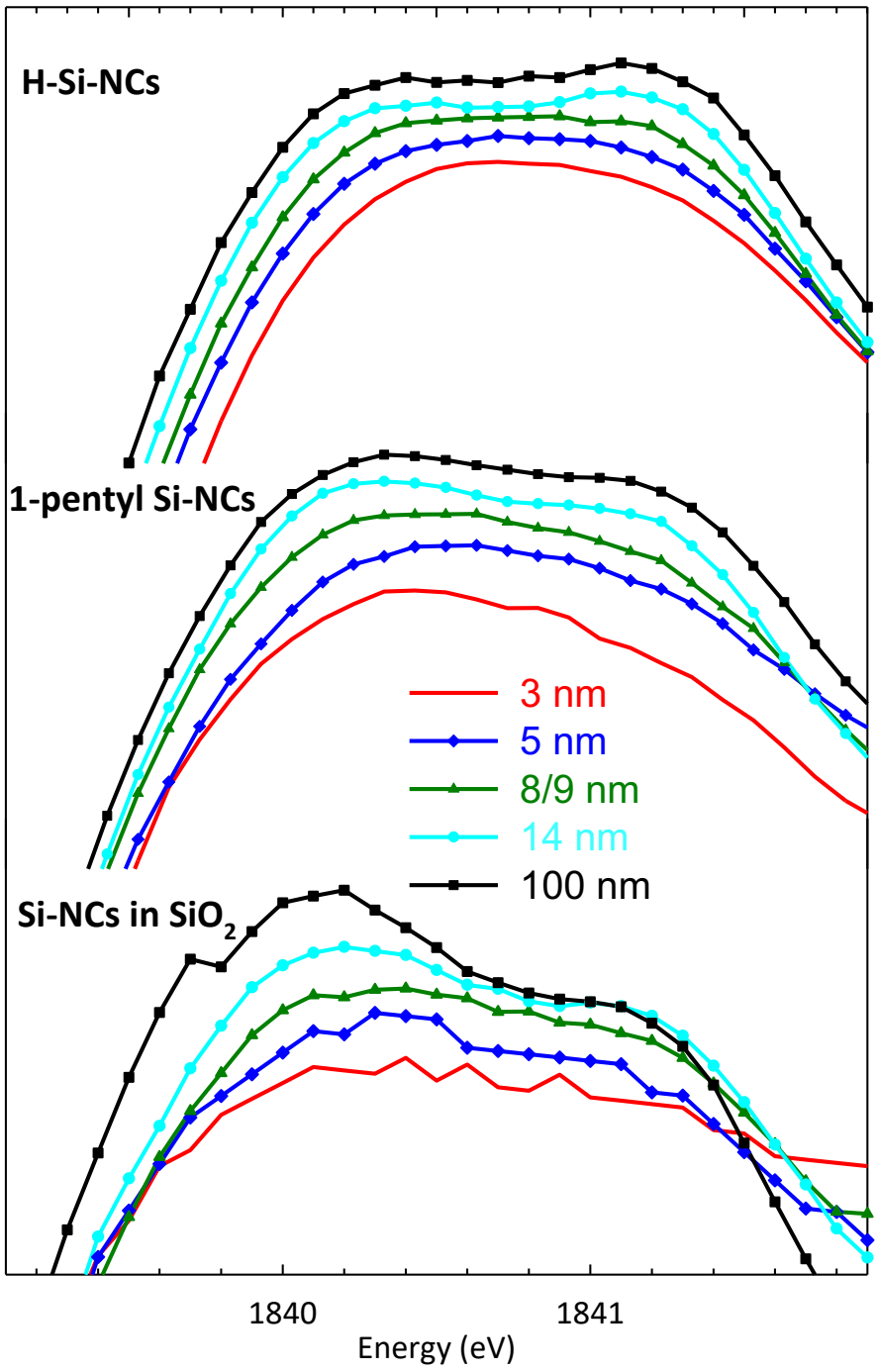

Figure 2: Magnification of the 'rabbit ear' feature in the silicon 1s NEXAFS spectra of hydrogen terminated silicon nanocrystals (top; H-Si-NCs), 1-pentyl terminated silicon nanocrystals (middle: 1-pentyl Si-NCs) and oxide embedded silicon nanocrystals (bottom; Si-NCs in SiO_2), of various diameter (3 nm, 5 nm, 8-9 nm, 14 nm and 100 nm). Spectra have been offset for clarity.

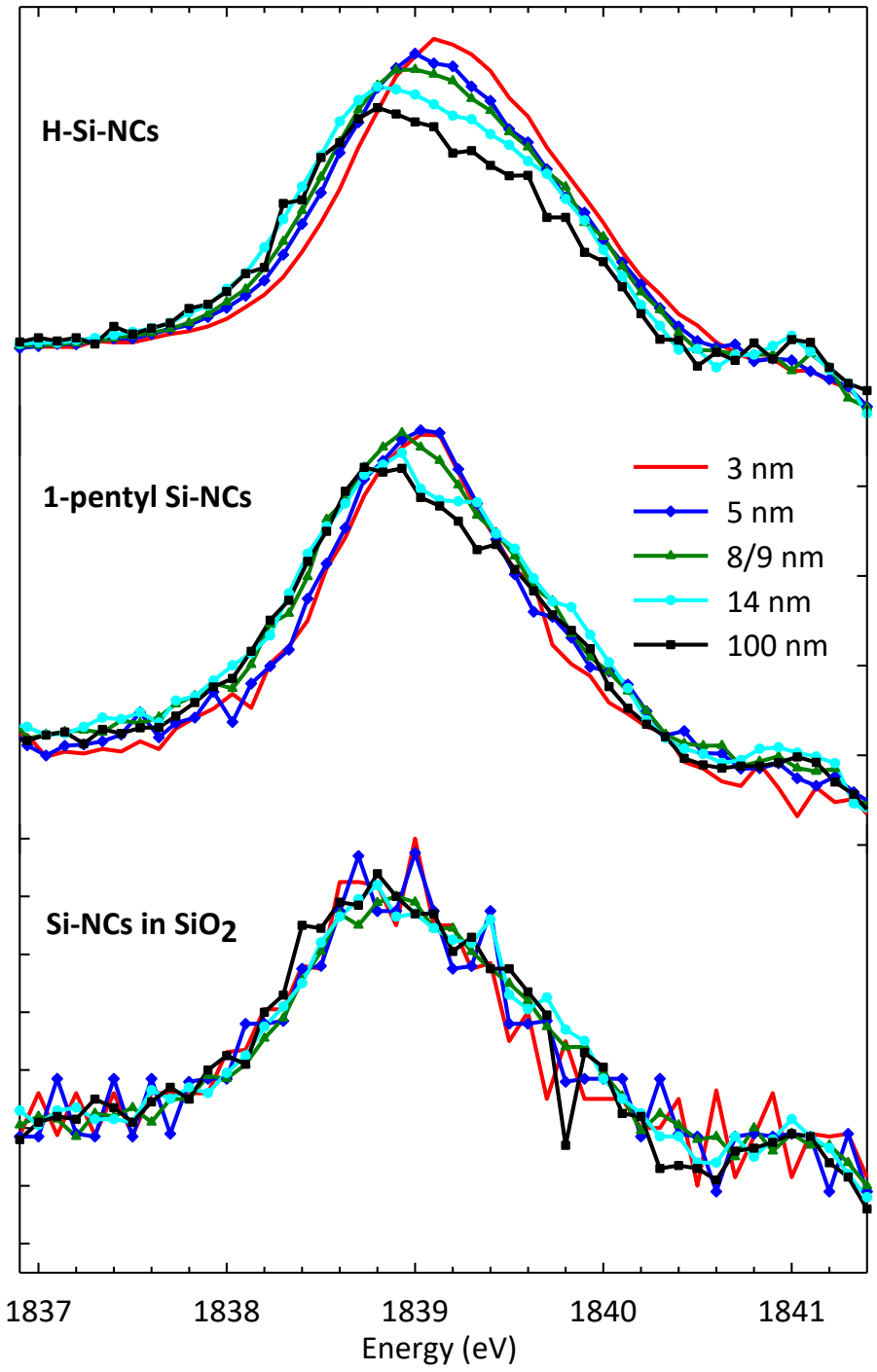

Figure 3: (left) Derivative of the silicon 1s NEXAFS spectra of hydrogen terminated silicon nanocrystals (top; H-Si-NCs), 1-pentyl terminated silicon nanocrystals (middle: 1-pentyl Si-NCs) and oxide embedded silicon nanocrystals (bottom; Si-NCs in SiO_2), of various diameter (3 nm, 5 nm, 8-9 nm, 14 nm and 100 nm).

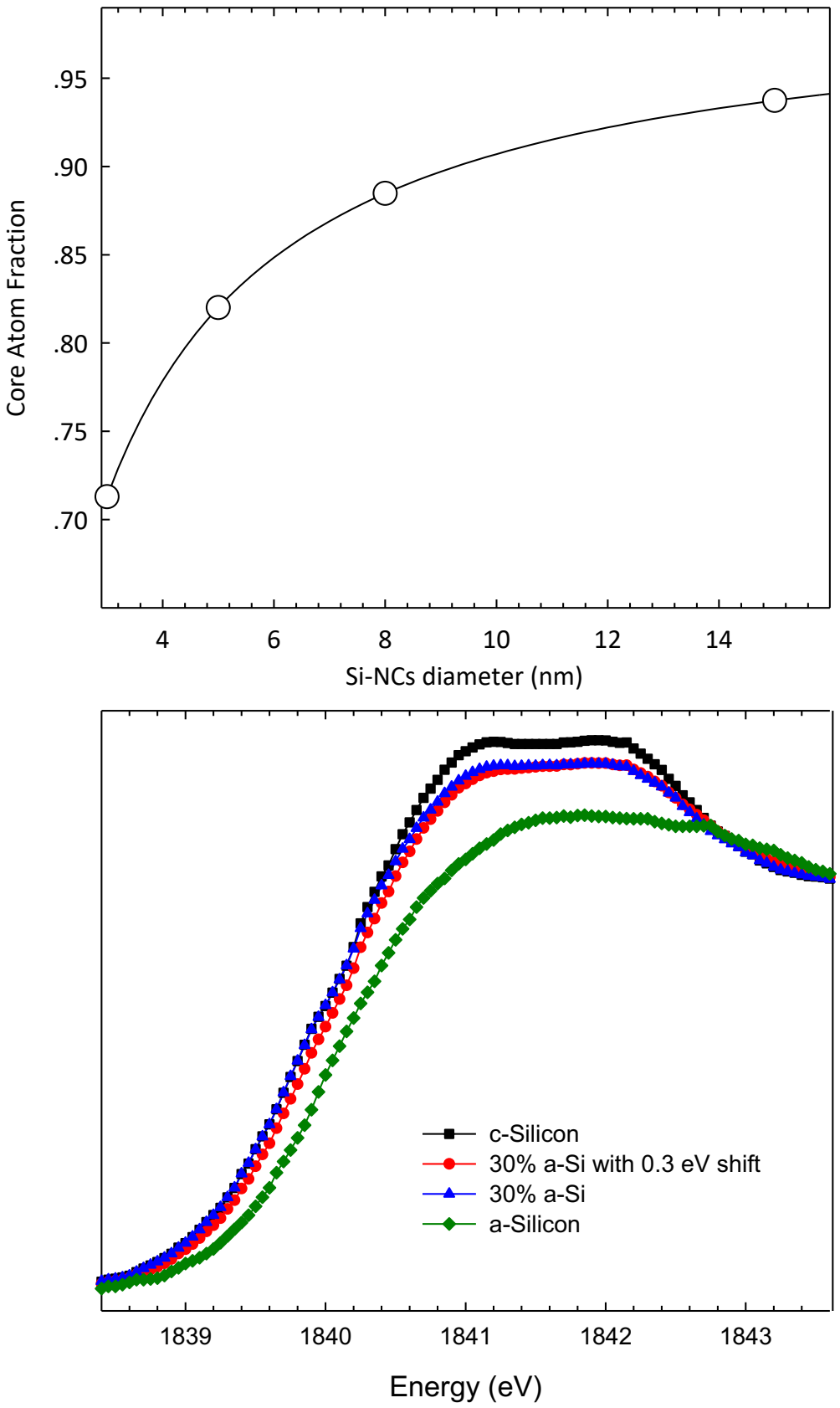

Figure 4: (top) Surface to Bulk ratios in Si-NCs as a function of NC diameter, for Si-NCs with a 1.6 Å shell thickness. The circles represent Si-NCs diameters examined in this work.(bottom) Simulation of the silicon 1s NEXAFS spectra of crystalline silicon with a 30% amorphous component and with a 0.3 eV shifted 30% amorphous content. Crystalline silicon (c-Si) and amorphous silicon (a-Si) spectra digitised from ref. x.